

# Multiple glass transitions in star polymer mixtures: Insights from theory and simulations

Christian Mayer,<sup>1,2</sup> Francesco Sciortino,<sup>1</sup> Christos N. Likos,<sup>2,3,4</sup>  
Piero Tartaglia,<sup>5</sup> Hartmut Löwen,<sup>2</sup> and Emanuela Zaccarelli<sup>1</sup>

<sup>1</sup>*Dipartimento di Fisica and CNR-INFM-SOFT, Università di Roma La Sapienza, Piazzale Aldo Moro 2, I-00185 Rome, Italy*

<sup>2</sup>*Institut für Theoretische Physik II: Weiche Materie,*

*Heinrich-Heine-Universität Düsseldorf, Universitätsstraße 1, D-40225 Düsseldorf, Germany*

<sup>3</sup>*The Erwin Schrödinger International Institute for Mathematical Physics (ESI), Boltzmannngasse 9, A-1090 Vienna, Austria*

<sup>4</sup>*Institut für Theoretische Physik, Technische Universität Wien,*

*Wiedner Hauptstraße 8-10, A-1040 Wien, Austria*

<sup>5</sup>*Dipartimento di Fisica and CNR-INFM-SMC, Università di Roma La Sapienza, Piazzale Aldo Moro 2, I-00185 Rome, Italy*

(Dated: October 27, 2018)

The glass transition in binary mixtures of star polymers is studied by mode coupling theory and extensive molecular dynamics computer simulations. In particular, we have explored vitrification in the parameter space of size asymmetry  $\delta$  and concentration  $\rho_2$  of the small star polymers at fixed concentration of the large ones. Depending on the choice of parameters, three different glassy states are identified: a single glass of big polymers at low  $\delta$  and low  $\rho_2$ , a double glass at high  $\delta$  and low  $\rho_2$ , and a novel double glass at high  $\rho_2$  and high  $\delta$  which is characterized by a strong localization of the small particles. At low  $\delta$  and high  $\rho_2$  there is a competition between vitrification and phase separation. Centered in the  $(\delta, \rho_2)$ -plane, a liquid lake shows up revealing reentrant glass formation. We compare the behavior of the dynamical density correlators with the predictions of the theory and find remarkable agreement between the two.

## I. INTRODUCTION

The slowing down of the dynamics in a supercooled liquid near the kinetic glass transition still requires a complete molecular understanding though recent progress has been made by experiments [1, 2, 3], by computer simulations [4, 5, 6, 7, 8, 9] and theory [10, 11, 12, 13]. The inherent polydispersity of colloidal systems facilitates the formation of disordered arrested states, as compared to the formation of the underlying equilibrium crystal [1]. In simulations, it is difficult to vitrify a pure one-component system of spherical particles due to the onset of crystallization, so that binary mixtures constitute a much richer and more convenient system to study the glass transition [14]. The thermodynamically stable state of an homogeneous undercooled binary melt typically involves two phase-separated binary crystals, A-rich and B-rich [15, 16] or a complex alloy in which the two components are mixed [15, 17]. In either case, the processes involved to reach true thermodynamic equilibrium require collective, mutually coordinated motions that take enormously long time. Therefore, the glass transition does take place also in simulation, since crystallization is prevented by the inherent polydispersity of the mixture. Hence, either binary or polydisperse systems have always been used as prototype models for the glass transition, for example repulsive soft spheres [4, 18, 19] or Lennard-Jones mixtures [20, 21, 22], charged mixtures [23], hard spheres [24], and Yukawa systems [25, 26]. In fact, the main reason for considering these *slightly asymmetric* binary mixtures is that crystallization was avoided. Upon cooling down typically all species freeze into a glass at the same temperature.

More recently, insight has been gained into the glass transition of *strongly asymmetric* mixtures consisting of

large colloidal spheres and small additives such as smaller colloids or non-adsorbing polymers which induce an effective depletion attraction between the large particles whose range is dictated by the size of the small particles. For strong asymmetries, very short range attractions (relative to the core size of the large particles) can thus be realized. A new type of glass was observed for these attractive interactions — termed an *attractive glass* — in experiments of colloid-polymer mixtures [27] and in computer simulations [28], following predictions based on mode coupling theory [29]. There is an interesting reentrant behavior [30] for increasing concentration of the additives: the *repulsive glass* (at vanishing additive concentration, i.e. in the absence of any attraction) melts upon a threshold additive concentration. The resulting melt revitrifies into a second type of glass, namely the *attractive glass*, for higher additive concentrations. Both for repulsive and attractive glass, only the large particles freeze into a disordered glassy matrix while the small additives always remain mobile and stay in a fluid state occupying the “holes” within the glassy matrix. This has been made explicit by computer simulations and mode coupling theory for the Asakura-Oosawa model in which the polymer-polymer interaction is assumed to be ideal. It was found [31] that the bare mobility of the additives is very important: when it is comparable to that of the colloids there is a freezing into a common glassy matrix of colloids and additives, while when it is much larger than the one of the colloids, freezing involves only the colloid component.

Experiments on binary hard sphere mixtures [32] have shown that there is a geometrically-inspired cross-over behavior in the dynamics of the small spheres when the ratio  $\delta$  of the two spheres diameter is about 0.15. This is

well below the size asymmetry considered in earlier mode-coupling calculations [33]. Another system in which dynamical arrest has been studied theoretically and experimentally are star polymers and micellar solutions [34, 35, 36, 37]. The first systematic attempt to vary the size asymmetry and to monitor its influence on the glass transition was performed in a binary mixture of star polymers in a good solvent [38]. Mode coupling theory and experimental data were compared for different size ratios  $\delta$  of the star polymer species. At low  $\delta$  the small additives remain ergodic in the glassy matrix formed by the large stars (*single glass*) while at high  $\delta$  both species become arrested simultaneously (*double glass*).

For increasing concentration of the smaller star polymers a melting into a fluid was found. The threshold concentration of the smaller stars for melting behaves non-monotonically as a function of  $\delta$  for fixed concentration of the big stars with a *U*-type shape. This non-monotonicity is a result of the ultrasoft effective interactions between the star polymers [39] and has no counterpart in hard-sphere based systems. Additive induced melting has also been found in mixtures of star polymers and linear polymer chains [40, 41]. More recently, a detailed study of the structural properties at high densities of the additives was performed [42] and an additional double glass, called *asymmetric glass*, has been identified.

In the present paper we elaborate more on the system of binary star polymers. Our motivation to do so is twofold: Firstly, aiming at a deeper understanding of the full dynamical behavior of collective- and self-correlations close to the various glass transitions, we performed extensive molecular dynamics computer simulations and compared the results with predictions of Mode Coupling Theory calculations. In this fashion, we were able to extract the dynamical scaling laws by fitting the simulation data. As regards the arrested plateau values of the dynamical correlations and localization lengths of both large and small components we find quantitative agreement between simulations and MCT. Secondly, we have expanded the parameter space up to concentrations of added small stars higher than previously studied [38] and found a reentrant vitrification of the molten state [42]. In the plane of size asymmetry  $\delta$  and added concentration  $\rho_2$  the molten state forms a lake with an *O*-shape. In addition to the asymmetric glass, we also observe an attractive glass at low  $\delta$  and high  $\rho_2$ , which is unstable with respect to phase separation.

The paper is organized as follows: in Sec. II we introduce the theoretical methods used in this paper. Sec. III contains the results based on Mode Coupling Theory, where we distinguish four regions in the  $(\delta, \rho_2)$  plane. Simulation data for the glass transition line based on iso-diffusivity curves are presented in Sec. IV, whereas simulation data for the dynamical correlations in the four different regions are subsequently discussed in Sec. V. Finally, in Sec. VI we summarize and present our conclusions.

## II. THEORETICAL METHODS

We describe the system in terms of effective interactions between the star centers [39]. The monomer degrees of freedom have been traced out in this approach. This method is applicable to the problem at hand, because we are interested in the arrest of the stars as whole objects and not in the arrest of the monomers themselves, which occurs at much higher concentrations. Concomitantly, the monomers maintain their fluctuating nature throughout. However, possible entanglements of the arms are not included in this description. The effective interaction between star centers depends parametrically on the number of arms (or functionality)  $f$ , and shows a logarithmic divergence when the two stars overlap within their corona diameters  $\sigma_i$ ,  $i = 1, 2$ , (where  $\sigma \cong R_h$  [40], with  $R_h$  the hydrodynamic radius), followed by a Yukawa-tail for larger separations [39].

In this work we study binary star mixtures with functionalities  $f_1 = 263$  and  $f_2 = 64$ . We express the mixture composition by quoting the values  $\rho_1 \sigma_1^3$  of the big and  $\rho_2 \sigma_2^3$  of the small stars, where  $\rho_i$ ,  $i = 1, 2$  are the respective number densities. The size ratio  $\delta = \sigma_2/\sigma_1$  is an additional parameter of the mixture. The two-component generalization of the aforementioned effective star-star potential reads [43],

$$\beta V_{ij} = \Theta_{ij} \times \begin{cases} -\ln\left(\frac{r}{\sigma_{ij}}\right) + \frac{1}{1 + \sigma_{ij}\kappa_{ij}} & \text{for } r \leq \sigma_{ij}; \\ \frac{1}{1 + \sigma_{ij}\kappa_{ij}} \left(\frac{\sigma_{ij}}{r}\right) \exp(\sigma_{ij}\kappa_{ij} - r\kappa_{ij}) & \text{else,} \end{cases} \quad (1)$$

where  $\sigma_{ij} = (\sigma_i + \sigma_j)/2$ ,  $2/\kappa_{ij} = \sigma_i/\sqrt{f_i} + \sigma_j/\sqrt{f_j}$  and

$$\Theta_{ij} = \frac{5}{36} \frac{1}{\sqrt{2} - 1} \left[ (f_i + f_j)^{3/2} - (f_i^{3/2} + f_j^{3/2}) \right]. \quad (2)$$

In order to calculate the fluid structure of the mixture we solve the binary Ornstein-Zernike (OZ) equation [44] with the Rogers-Young (RY) closure [45]. This amounts to postulating the additional relation to hold between the total correlation functions  $h_{ij}(r)$  and their direct counterparts  $c_{ij}(r)$ :

$$h_{ij}(r) = \exp[-\beta V_{ij}(r)] \times \left[ 1 + \frac{\exp[(h_{ij}(r) - c_{ij}(r))f(r)] - 1}{f(r)} \right] - 1, \quad (3)$$

where  $f(r) = 1 - \exp(-\alpha r)$  with  $(\alpha > 0)$ . The value of the parameter  $\alpha$  is determined by requiring the equality of the ‘fluctuation’ and ‘virial’ total compressibilities of the system [45, 46]. For  $\alpha \rightarrow 0$  the Percus-Yevick closure is obtained, while for  $\alpha \rightarrow \infty$  the hypernetted chain closure (HNC) is recovered [44]. The RY closure has been shown to correctly describe liquid properties for a number of repulsive potentials, including star polymers [47], spherical ramp [48] and square shoulder [49] potentials.

From solving the OZ equation, it is also possible to calculate the partial static structure factors, describing the density correlators at equal time,

$$S_{ij}(q) = \delta_{ij} + \sqrt{\rho_i \rho_j} \tilde{h}_{ij}(q) = \frac{1}{\sqrt{N_i N_j}} \langle \rho_i^*(\mathbf{q}, 0) \rho_j(\mathbf{q}, 0) \rangle \quad (4)$$

where  $\tilde{h}_{ij}(q)$  denotes the Fourier transform of the total correlation function and

$$\rho_j(\mathbf{q}, t) = \sum_{l=1}^{N_j} \exp \left[ i \mathbf{q} \cdot \mathbf{r}_l^{(j)}(t) \right],$$

with  $\mathbf{r}_l^{(j)}$  being the coordinates of the  $l$ -th particle of species  $j$  ( $j = 1, 2$ ) and the asterisk denoting the complex conjugate. The partial static structure factors calculated within RY approximation for binary star polymer mixtures have been found in very good agreement with those obtained by simulations employing the effective potential of Eq. (1) [50].

Our theoretical study of the glass transition is based on the ideal Mode Coupling Theory (MCT), a theory that describes the time evolution of the density autocorrelation functions, starting only from the knowledge of the static structure factors, via a set of coupled integro-differential equation [10]. The normalized time-dependent collective density autocorrelation functions are defined as,

$$\phi_{ij}(q, t) = \langle \rho_i^*(\mathbf{q}, 0) \rho_j(\mathbf{q}, t) \rangle / \langle \rho_i^*(\mathbf{q}, 0) \rho_j(\mathbf{q}, 0) \rangle. \quad (5)$$

It is also useful to focus on the self part of the density correlation functions, which describes the dynamics of a tagged particle,

$$\phi_j^s(q, t) = \left\langle \sum_{l=1}^{N_j} \exp \left\{ i \mathbf{q} \cdot \left[ \mathbf{r}_l^{(j)}(t) - \mathbf{r}_l^{(j)}(0) \right] \right\} \right\rangle. \quad (6)$$

The long-time limit values of  $\phi_{ij}(q, t)$ , i.e. the partial non-ergodicity factors, respectively for the collective and self correlation functions, are defined as,

$$f_{ij}(q) = \lim_{t \rightarrow \infty} \phi_{ij}(q, t) \quad (7)$$

$$f_j^s(q) = \lim_{t \rightarrow \infty} \phi_j^s(q, t). \quad (8)$$

A glass transition is identified within MCT as an ergodic to non-ergodic transition, when the non-ergodicity factor discontinuously jumps from zero, typical of a fluid, to a finite value typical of a glass [10].

In binary mixtures with large size asymmetries, there is a vast separation of time-scales between large (species 1) and small (species 2) stars due to the enormous difference in mobilities. Therefore we can use one-component MCT for the large stars only, and solve the equation for the non-ergodicity parameter  $f_{11}(q)$  [31],

$$\frac{f_{11}(q)}{1 - f_{11}(q)} = \frac{1}{2} \int \frac{d^3 k}{(2\pi)^3} V(\mathbf{q}, \mathbf{k}) f_{11}(k) f_{11}(|\mathbf{q} - \mathbf{k}|), \quad (9)$$

with

$$V(\mathbf{q}, \mathbf{k}) = \frac{\rho_1}{q^4} [\mathbf{q} \cdot (\mathbf{q} - \mathbf{k}) \tilde{c}_{11}(|\mathbf{q} - \mathbf{k}|) + \mathbf{q} \cdot \mathbf{k} \tilde{c}_{11}(k)]^2 \times S_{11}(q) S_{11}(k) S_{11}(|\mathbf{q} - \mathbf{k}|), \quad (10)$$

The solution with the largest  $f_{11}(q)$  is the long-time limit [10] of the density correlators. We note here that, in the one-component effective treatment, we use  $S_{11}(q)$  calculated from solving the binary OZ equation within RY closure, arising from the full binary interactions of Eq. (1). In this respect, we are treating the small stars as an effective medium, and their influence on the interactions between the large stars is taken into account explicitly and not through an effective one-component picture [46].

MCT assumes a vast separation of time scales between the slow and fast degrees of freedom. For small size asymmetries, the separation of timescales between the different star species decreases and one-component MCT cannot be used [31]. In the general case of a mixture, when relaxation time-scales of the two species are comparable, the long-time MCT equations (Eq. 9) are easily generalized [19, 51] in terms of matrices as,

$$\bar{\mathbf{f}}(q) = \bar{\mathbf{S}}(q) - \{ \bar{\mathbf{S}}(q)^{-1} + \mathcal{F}(\bar{\mathbf{f}}, q) \}^{-1}, \quad (11)$$

where  $\bar{\mathbf{S}}(q) = \sqrt{x_i x_j} S_{ij}(q)$ , with  $x_i = N_i / (N_1 + N_2)$  being the number concentration of species  $i$ .

The functional  $\mathcal{F}(\bar{\mathbf{f}}, q)$  is defined as

$$\mathcal{F}_{ij}(\bar{\mathbf{f}}, q) = \frac{1}{2q^2} \frac{\rho}{x_i x_j} \sum_{mm'n'} \int \frac{d^3 k}{(2\pi)^3} V_{imm'}(\mathbf{q}, \mathbf{k}) \times f_{mn}(k) f_{m'n'}(p) V_{jn'n'}(\mathbf{q}, \mathbf{k}), \quad (12)$$

with  $\rho = \rho_1 + \rho_2$  and  $p = |\mathbf{q} - \mathbf{k}|$ . The vertices  $V_{imm'}(\mathbf{q}, \mathbf{k})$  depend on the equilibrium structure of the system and are given by

$$V_{imm'}(\mathbf{q}, \mathbf{k}) = \frac{\mathbf{q} \cdot \mathbf{k}}{q} \tilde{c}_{im}(k) \delta_{im'} + \frac{\mathbf{q} \cdot (\mathbf{q} - \mathbf{k})}{q} \tilde{c}_{im'}(|\mathbf{q} - \mathbf{k}|) \delta_{im}.$$

In the case of binary or multicomponent MCT, the theory predicts, through the couplings between species in Eq. (11) a simultaneous jump from zero to a finite value for all partial collective non-ergodicity parameters  $f_{ij}(q)$ . However, this does not hold for the self part  $f_i^s(q)$ , for which the equations are [52],

$$K_i(q) = \frac{1}{\rho_i q^2} \sum_{j,k} \int \frac{d^3 q'}{(2\pi)^3} f_i^s(|\mathbf{q} - \mathbf{q}'|) \tilde{c}_{ij}(q') \tilde{c}_{ik}(q') \times \sqrt{S_{jj}(q') S_{kk}(q') f_{jk}(q')}, \quad (13)$$

where

$$f_i^s(q) = \frac{1}{1 + q^2 / K_i(q)}, \quad (14)$$

so that it is possible to distinguish also the case of mobile particles in a frozen environment, for example for the small stars in our case, when  $f_{22}(q) \neq 0$  but  $f_2^s(q) = 0$  [52, 53].

In general multiple glassy solutions of Eq. (12) can exist, due to higher order bifurcation singularities. This case has been extensively studied for effective one-component systems of attractive colloids, where higher order MCT singularities have been predicted theoretically [54] and verified by numerical simulations [55, 56] and experiments [27, 57, 58]. For multicomponent systems, calculations of MCT higher order singularities have not been reported so far. However, hints of the presence of such higher order singularities and glass-glass transitions, in particular of one of the involved species, have emerged in simulations of asymmetric polymer blends and soft sphere mixtures [59, 60, 61]. In the case of distinct glassy states, the non-ergodic properties of the various arrested states will be different from one another, a feature that will be reflected on the corresponding non-ergodicity factors  $f_{ij}(q, t)$ . Also, close to such singularities, competition between the different glassy states modifies the standard MCT dynamical behavior close to the liquid-glass transition (labeled usually of type  $B$  or  $A_2$ ). For such an  $A_2$  transition, a two-step relaxation is well described by MCT, through an asymptotic study of the correlators near the ideal glass solutions.

For a generic density correlator  $\phi$  in the liquid the critical non-ergodicity parameters  $f^c(q)$  can be extracted. The departure from the plateau, i.e. the start of the  $\alpha$ -process, is described by a power law, called the von Schweidler law, regulated by the characteristic exponent  $b$ , which is independent of the particular  $q$ -vector considered,

$$\phi(q, t) - f^c(q) \sim -h^{(1)}(q)(t/\tau_0)^b + h^{(2)}(q)(t/\tau_0)^{2b} \quad (15)$$

with  $\tau_0$  being the characteristic time of the relaxation. The quantities  $h^{(1)}(q)$  and  $h^{(2)}(q)$  are referred to respectively as critical amplitude and correction amplitude [10]. The  $\alpha$ -relaxation process can also be well described by a stretched exponential, i.e.

$$\phi(q, t) = A(q) \exp[-(t/\tau_q)^{\beta_q}] \quad (16)$$

where the amplitude  $A(q)$  determines the plateau value, and the stretching exponent  $\beta_q \leq 1$ . For large  $q$  values, it has been shown that  $\beta_q \rightarrow b$  [62]. The von Schweidler exponent  $b$  is related to another important MCT parameter, named the exponent parameter  $\lambda$ [10]. This includes all information on the dynamics of the systems on approaching the MCT transition. It takes values in the interval  $1/2 < \lambda \leq 1$ .

Close to higher order singularities, the dynamical behavior is predicted to obey a logarithmic behavior and  $\lambda$  should approach 1. In particular, it holds,

$$\phi(q, t) \sim f^c(q) - h(q) \left[ B^{(1)} \ln(t/\tau) + B_q^{(2)} \ln^2(t/\tau) \right]. \quad (17)$$

We define  $q^*$  as the wave-number at which the correlators decay purely logarithmically, that is  $B_{q^*}^{(2)} = 0$ . Here  $\tau$  stands for a time-scale which diverges if the state approaches the mathematical singularity. The formula is obtained by asymptotic solution of the MCT equations [63]. The first term  $f^c(q)$  is the sum of the non-ergodicity parameter at the singularity plus a correction which depends on the distance from the singularity.

We will use Eq. (15)–(17) to describe the the correlators  $\phi_{11}(q, t)$  and  $\phi_{22}(q, t)$  independently. In the following, for those states where the density correlators do not follow power-laws or stretched exponentials, we adopt the expression in Eq. (17) to extract the non-ergodicity parameters from the simulations and find that they are indeed very well described by that function.

### III. MCT RESULTS

Following the experimental setup discussed in [38], we investigate the effect of the addition of a second component of varying size and concentration on the glass formed by the one-component large stars with  $f_1 = 263$ . As we have shown before [38], the qualitative trends do not depend on details of the mixture properties, therefore we consider only  $f_2 = 64$  in this work. We commence from a glass of large stars only, with a fixed density  $\rho_1 \sigma_1^3 = 0.345$ , corresponding to a glassy state within MCT [34]. At this state point, we add small stars and study the stability of the large star glass [75].

From the MCT analysis, we determine a glass transition diagram in the  $(\delta, \rho_2)$  plane (see Figure 1). Results obtained both in the full binary treatment of the mixture and in the effective one-component representation are shown. With respect to the  $(\rho, T)$  phase diagrams that are usually shown in colloid-polymer (CP) mixtures [27], we focus here on a single isochore and consider the addition of small stars of different sizes and concentrations.

Examining Fig. 1, a liquid region is found, being surrounded by many different glasses. We detect a reentrant behavior on increasing the density of additives both for small and large sizes of additives as well as a reentrance in size ratio. For convenience, we can roughly divide the phase diagram of star-star mixtures in four different regions to be discussed in the following:

1. small size and small concentration of the additives (region I): single glass;
2. large size and small concentration of the additives (region II): double glass;
3. large size and large concentration of the additives (region III): asymmetric glass;
4. small size and large concentration of the additives (region IV): attractive glass/phase separation.

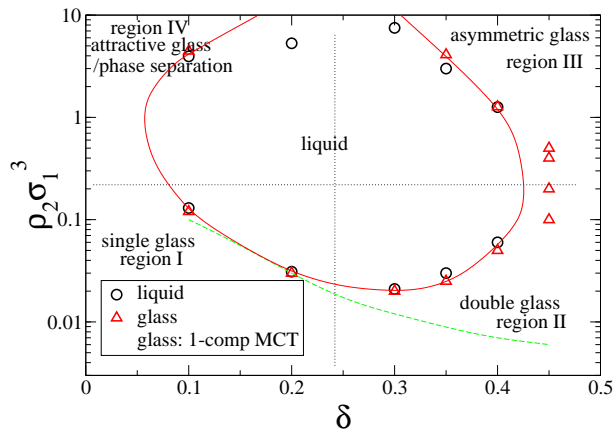


FIG. 1: Ideal MCT kinetic phase diagram in the size ratio-additive density plane. Symbols are the bracketing state points for the ideal-glass transition, determined by using the two-component MCT. The full line through the points is a guide to the eye. The dashed line is the ideal-glass line calculated on the basis of the one-component MCT. Four different regions with glassy states can be identified: we name them respectively single glass (region I), double glass (region II), asymmetric glass (region III) and attractive glass/phase separated glass (region IV). These calculations refer to the case  $\rho_1 \sigma_1^3 = 0.345$ . The dotted lines roughly separate the different regions of the phase diagram.

Preliminary information on the single, double and asymmetric glasses have been reported in Ref. [38, 42]. Here we summarize the most important aspects for completeness. We start by examining region I. The small stars always remain liquid in this regime, even in those states in which the large ones are arrested (single glass) [38]. The addition of small stars with size ratio up to  $\delta \approx 0.25$  causes the large glass star to melt due to a depletion-induced softening of the repulsions with respect to the one-component case [46], weakening the stability of the cages [38].

On the other hand, moving into region II by increasing the small stars diameter, the addition of a second component of stars with  $0.25 \lesssim \delta \lesssim 0.45$  leads to a glassy state formed by both components (double glass) [38]. Here, an increase of  $\rho_2$  also melts the glass but through an entirely different mechanism, found in MCT and also confirmed by experiments [38]. Indeed, the glass becomes stiffer through the addition of a second glassy component, as shown by the growth of the elastic modulus in theory and experiments reported in [38, 50] up to the melting density. At this point, it becomes entropically more convenient to free available volume for both stars simultaneously, which amounts to a finite energetic increase, sufficient to cause liquification. Therefore, this melting mechanism is only possible through the softness of interactions involved, and it does not have an equivalent in terms of hard-sphere mixtures. We note, that the presence of two different glasses for asymmetric mixtures, a single to a double glass, depending on the size ratio, was

already found for hard spheres [32, 52, 53], but the new feature of the presently investigated soft mixtures is that both glasses can be simultaneously melted by increasing the amount of the small additives in the mixture.

Clearly, a theoretical framework capable to correctly describe the single glass should be based on the slowing down of the large stars only, i.e. one-component MCT, where the smaller stars are assumed to form a fluid medium that does not participate in the glass formation, is the conceptually right framework to use. On the other hand, in the double glass both species become comparably slow, thus compelling the use of binary MCT. It turns out that in the case of star polymers mixtures, differently from that of colloid-polymer mixtures [31], at low  $\delta$ , i.e., in the single glass regime, both treatments give qualitatively the same behavior, as illustrated also in Figure 1, while at large  $\delta$ , in the double glass regime, the discrepancy becomes large, signaling the tendency of the small component to also arrest. Only binary MCT can be used in this region, giving rise to the U-shape also observed in the experiments for low  $\rho_2$  [38]. Hence, in the following we just refer to two-component MCT in all regions, unless explicitly mentioned.

In the present work we complement previous results [38, 50] with the investigation of Regions III and IV. In region III, for large concentration of additives with  $\delta \sim 0.4$ , we find a reentrant vitrification with respect to  $\rho_2$ , with the appearance of a new glassy state with smaller localization length for large  $\delta$  and large  $\rho_2$ . Due to the softness of the interactions local rearrangements take place which leads to a change of coordination of the large stars as well as to an asymmetric deformation of the cages [42]. The increase of  $\rho_2$  causes a second jamming at a new length scale that will depend on the particular parameters of the mixture.

Finally in region IV, at low  $\delta$ , the depletion mechanism induces effective attractions between the large stars [46], causing phase separation. Phase separation is accompanied by an increase of the structure factor at infinite wavelength, and a blind use of it in the mode-coupling equations would predict glass formation driven by the small wavevectors. However, with the use of RY structure factors, we are only able to find a glass within binary MCT for  $\delta = 0.1$ , while the one-component treatment always provides a liquid state up to the maximum investigated  $\rho_2$  approaching phase separation. We could not extend the analysis to larger  $\rho_2$  due to a breakdown in the convergence of the Rogers-Young closure, as well as the simplest HNC closure in this region, a possible sign of a close thermodynamic instability.

In addition to the phase diagram, we report in Fig. 2 the calculated MCT partial non-ergodicity parameters, both for self [Fig. 2(a-b)] and collective [Fig. 2(c-d)] relaxation dynamics for  $\delta = 0.1$  and  $\delta = 0.4$ . Such results correspond to the glassy points closest to the transition, hence they are ‘critical’ non-ergodicity parameters. The small stars  $f_2^s(q)$  allows us to distinguish immediately a single from a double glass, since it is identically zero

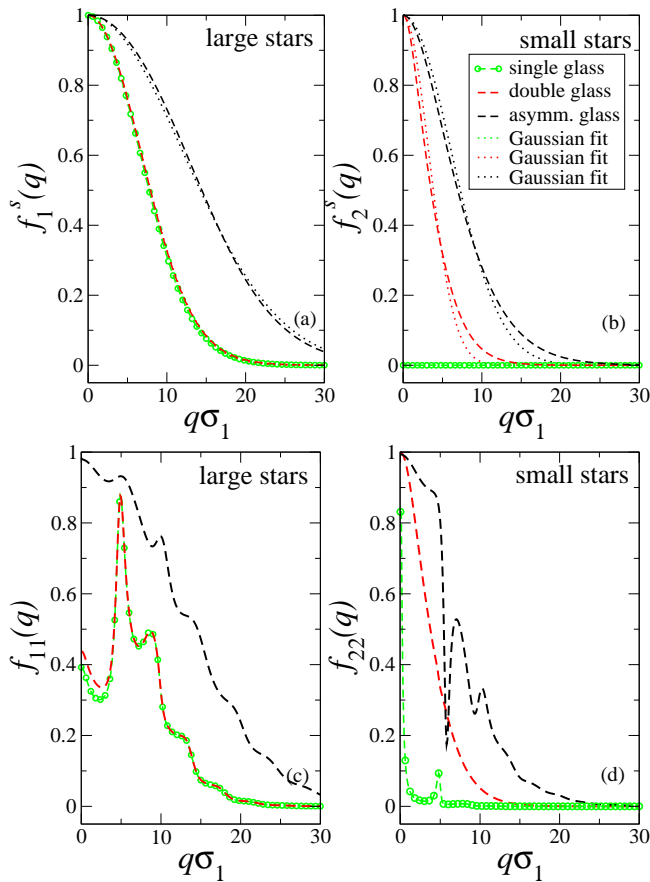


FIG. 2: Partial non-ergodicity parameters at the MCT transition. The (a) and (b) panels show respectively the large-star and small star components of the self non-ergodicity parameters for the three different glasses. They also show Gaussian fits (dotted lines), which allow us to extract the localization length. The  $f_1^s$  of the large stars in the single and double glass are virtually identical, therefore the lines fall on top of each other, while those for the small stars are very different in all three cases. In the (c) and (d) panels we show the non-ergodicity parameters for the collective dynamics. For all curves  $\rho_1\sigma_1^3 = 0.345$ . For the single glass  $\rho_2\sigma_1^3 = 0.12$  and  $\delta = 0.1$ , while in the double glass  $\rho_2\sigma_1^3 = 0.05$  and  $\delta = 0.4$ . The asymmetric glass corresponds to  $\rho_2\sigma_1^3 = 1.27$  and  $\delta = 0.4$ .

for the single glass, as already found in binary asymmetric hard sphere mixtures [52]. Thus, although, in binary MCT the broken ergodicity transition is postulated to happen simultaneously for both species, the self non-ergodicity parameter allows to distinguish between mobile and immobile species. Also, the partial  $f_i^s(q)$  for both types of stars have a larger width in the asymmetric glass than in the double glass. Fitting  $f_i^s(q)$  to a Gaussian curve  $\exp(-q^2/6l_{\text{MCT}}^2)$  provides an estimate for the localization length  $l_{\text{MCT}}$  within the glass. Fits are also reported in the figure. The Gaussian fit works very well for large stars, but deviations are observed for small stars, in both double and asymmetric glasses. The extracted localization length is  $l_{\text{MCT}} \approx 0.26\sigma_1$  for large stars both in single and double glass, while it is  $l_{\text{MCT}} \approx 0.14\sigma_1$

for the asymmetric glass, i.e., the cage size reduces by a factor of two. A larger variation in  $l_{\text{MCT}}$  is predicted for the small stars from  $0.51\sigma_1$  for the double glass at low  $\rho_2$  to  $0.11\sigma_1$  for the asymmetric glass at high  $\rho_2$ , a value which is almost identical to the one for the large stars in the same state. For the collective  $f_{ii}(q)$ , the results are very similar to those of the self non-ergodicity parameters, only much stronger oscillation peaks are observed in phase with the static structure factor. For the small stars, these appear only in the asymmetric glass regime. We notice that upon changes in  $\delta$  within the low  $\rho_2$  glasses, we detect no change in  $f_{11}(q)$  between single and double glass. However, a significant increase is observed for large  $\delta$ , upon increasing  $\rho_2$ , while approaching the asymmetric glass. This increase results in a more extended  $q$ -width in  $f_{11}(q)$ , a finding similar to that for attractive glasses in colloid-polymer mixtures, where further increase of the additives leads to an increase of the non-ergodicity parameter both in amplitude and range [28]. Therefore, in the asymmetric regime, a strong localizing mechanism is at hand, with some similarities to an effective attraction. However, looking at the partial  $S_{ij}(q)$  we do not see an increase in the compressibilities or a non-monotonic dependence in the growth of peaks. Simply, the structure factor peaks for large stars continue to decrease upon addition of small stars, while these display themselves more and more enhanced peaks. In [42], we have shown that the change of structure is accompanied by a dramatic decrease in the coordination number of the large stars and an asymmetric deformation of the large star cages.

Finally, an analysis of the MCT exponents reveals that, for both single and double glass,  $\lambda \simeq 0.71$  and  $b \simeq 0.625$ , the same result obtained for one-component star polymer solutions. However, we note that  $\lambda$  grows considerably close to the asymmetric glass transition. At the transition point corresponding to  $\delta = 0.4$ ,  $\lambda \sim 0.8$ , corresponding to a von Schweidler exponent  $b \sim 0.47$ .

#### IV. SIMULATIONS: NUMERICAL DETAILS

We performed standard Newtonian dynamics simulations for stars interacting via the effective potential in Eq. (1). Although the use of Brownian dynamics simulations would be more realistic for star-star mixtures to mimic the solvent effects, this is less efficient and it would not allow us to probe the full slow dynamics regime efficiently. Moreover, several confirmations of independence of long-time properties from microscopic dynamics have been provided so far [34, 65] for systems close to their glass line. We investigate several compositions, in order to have a complete picture of the phase diagram and of the dynamical slowing down. Due to the various compositions to be investigated, the number of particles varies throughout the diagram. In general, we fix  $N_1 = 1000$  and vary  $N_2$  accordingly. However, for  $\rho_2\sigma_1^3 \geq 10$ , we use  $N_1 = 250$ . Also, for  $\rho_2\sigma_1^3 \leq 0.1$ , i.e. in single and dou-

ble glass regimes, we fix the minimum number of small particles to  $N_2 = 500$  and vary  $N_1$  accordingly. We investigate  $f_1 = 263$  and  $f_2 = 64$ , the same values used in the MCT analysis. To improve statistics, we average over 5 independent runs for each studied state point.

In order to describe the dynamics of the system properly, we have to choose the short-time mobilities of the small particles with respect to the large ones. Following the ideas in [31], we use the scaling for the mass  $m$  typical of the star polymers, namely  $m \sim f^{2/3} \sigma^{5/3}$  [66, 67]. This results in a ratio between the small and large particles mass equal to  $m_2/m_1 = (f_2/f_1)^{2/3} \delta^{5/3}$ . Note that a physical choice of the small particle mass is crucial, since as already noticed in earlier simulations of explicit colloid-polymer mixtures [31], the addition of small particles of mass identical to the one of the large particles, has the result of further slowing down the large particle dynamics. This would imply no melting at any given  $\rho_2$  and  $\delta$  in contrast with MCT predictions and experimental results. Units of length, mass and energy are  $\sigma_1$ ,  $m_1$  and  $k_B T$ , respectively. Time is measured in  $\tau_{MD} = \sqrt{m_1 \sigma_1^2 / (k_B T)}$  and the integration time step is varied according to the mass ratio, as  $\delta\tau = 5 \cdot 10^{-3} \sqrt{m_2/m_1} \tau_{MD}$ .

We employ numerical simulations to (i) evaluate the iso-diffusivity lines in the  $\rho_2 - \delta$  plane and (ii) study specific features of the dynamics for selected state points approaching the four glass regions.

Simulations for the isodiffusivity lines are performed for  $\rho_1 \sigma_1^3 = 0.345$ . Note however that at this density the slowing down of the dynamics observed in the simulations is not very significant. To study the dynamics on approaching the glass transition(s) we have been forced to increase the density of the large particles to generate a slower dynamics. Indeed, similarly to other studied cases like that of hard spheres, a systematic shift of the MCT transition with respect to the slowing down taking place in experiments or simulations, is present. This shift usually applies in the direction of MCT anticipating the onset of glassy dynamics and our findings agree with this general picture.

Moreover, we have considered a small poly-dispersity in the large particles diameter. This is particularly important at low  $\rho_2$ , when the amount of small stars is not sufficient by itself to prevent crystallization of the large stars. We selected the value  $\rho_1 \sigma_1^3 = 0.41$  to investigate the dynamics of single and double glass respectively, while we retained the value  $\rho_1 \sigma_1^3 = 0.345$  for the asymmetric glass. The larger density and the absence of crystallization allows us to observe a slowing down of the dynamics for the large particles (even in the absence of additives), and consequently also the single and double glass. We employ a polydispersity in the large-stars diameter, chosen to follow a Gaussian distribution with a width of 10% [64].

We have checked that, compared to the one-component case, the dynamics are not affected. For the comparison, we have to account for the polydispersity in the

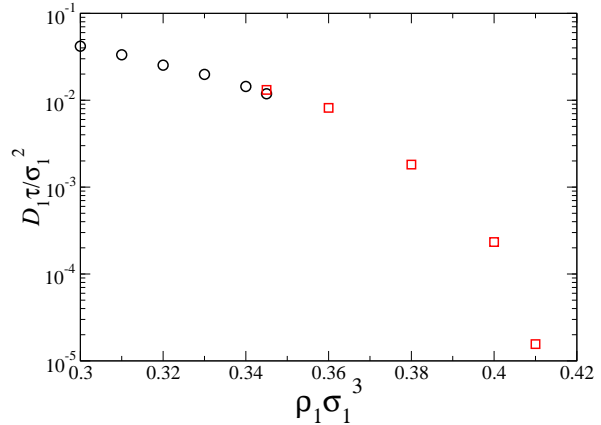


FIG. 3: Diffusivity of the one-component system as a function of star density. Circles correspond to the monodisperse system with  $f = 263$  and squares to simulations with added polydispersity to prevent the system from forming a crystal. The exploration of three orders of magnitude in  $D_1$  is thus possible.

right way when calculating the density, i.e. by matching the value  $\rho_1 \langle \sigma_1^3 \rangle$  with the corresponding one-component density. In this way, we can decrease the diffusivity by three orders of magnitude by increasing  $\rho_1$ , as illustrated in Figure 3, comparing results for the monodisperse and polydisperse one-component reference system.

Finally, for the simulations of the attractive glass, we have focused on monodisperse large stars, due to the absence of systematic crystallization in this case.

## V. SIMULATION: ISODIFFUSIVITY LINES

The iso-diffusivity lines are precursors of the glass transition lines, and they always display a similarity in shape as the MCT line, as demonstrated already for one-component star polymers [34], for other repulsive potentials [48], as well as for short-range attractive square well potentials [68].

To study iso-diffusivity lines we calculate the mean-squared displacement (MSD)  $\langle r_i^2(t) \rangle$  ( $i = 1, 2$ ) of large and small stars separately. From the long-time behavior, we extract the respective self-diffusion coefficient defined as, following the Einstein relation,  $D_i = \lim_{t \rightarrow \infty} \langle r_i^2(t) \rangle / (6t)$ .

In Fig. 4, we report the iso-diffusivity lines for three different values of  $D_1/D_0$  in the  $(\delta, \rho_2)$  plane, where  $D_0$  is the diffusion coefficient in the absence of small particles. The fact that we examine only a decade in decrease of  $D_1/D_0$  is due to the many constraints to study the whole phase diagram under very different mixture compositions. The line corresponding to the slowest states is drawn only on the large  $\delta$  side, because the diffusivity

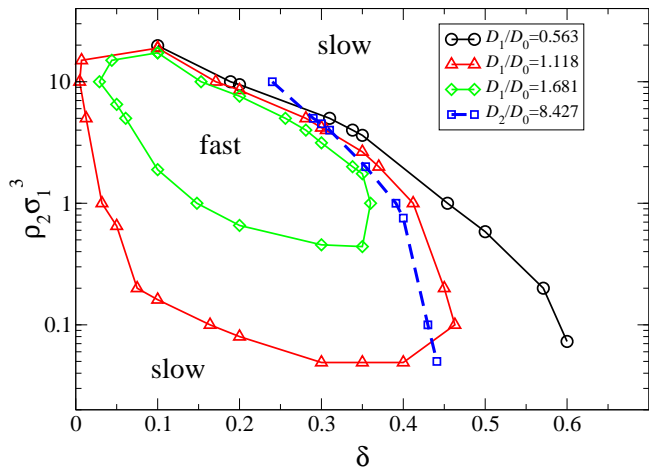


FIG. 4: Iso-diffusivity lines from MD simulations in the  $(\rho_2, \delta)$ -representation. The density of large stars is kept constant at  $\rho_1 \sigma_1^3 = 0.345$  and the large stars are monodisperse. The line for the smallest value of the diffusivity is not closed because the chosen value of  $D_1$  is smaller than the diffusivity of the reference one-component system ( $D_0$ ). The dashed curve is an isodiffusivity line of the small stars.

is lower than in the one-component system and therefore no closed loop exists for this value of  $D_1$ . Notwithstanding these details, the emergence of an asymmetric “O”, that resembles the shape of the MCT phase diagram, is evident. This was confirmed also for higher  $\rho_1$  [42], demonstrating that the topology does not depend on the precise value of  $\rho_1$  studied. Recently, this asymmetric “O” has been observed experimentally [42].

Additionally, from the simulations we can also trace out correctly the iso-diffusivity lines of the small stars (Fig. 4). Within binary MCT, there should be no distinction between the glass lines of the large and small stars, based on the assumption that small stars are as slow as the large stars. It has a similar shape as the large  $\delta$ /large  $\rho_2$  region. Note that the dynamics of the small stars is much faster for low  $\delta$ , where the mobility of the two species is very dissimilar, and hence the small star isodiffusivity lines do not show an “O” shape.

## VI. SIMULATION: MULTIPLE GLASSY STATES

We can now exploit the simulation results to directly probe the four regions of slowing down and compare the different glasses, in order to clarify the characteristics of the multiple glassy states appearing in these types of mixtures, in comparison with the MCT results.

### A. Region I: Single glass

We consider the state point  $\rho_1 = 0.41$ ,  $\rho_2 = 0.1$  and  $\delta = 0.1$  (2250 particles in the simulation box). The

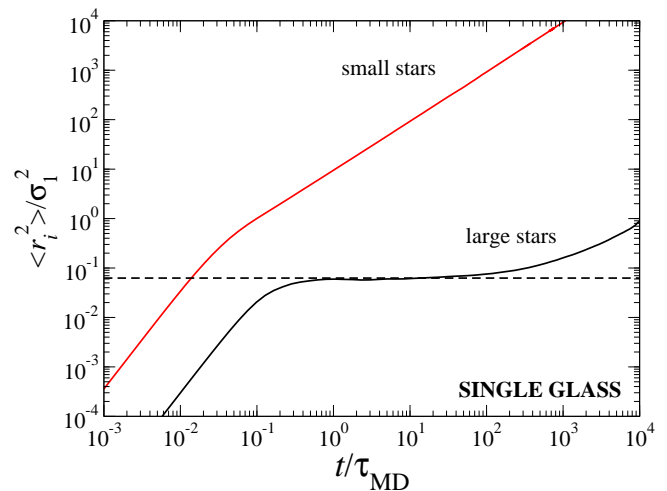


FIG. 5: Mean squared displacements for large and small stars in the single glass. The densities are  $\rho_1 \sigma_1^3 = 0.41$  and  $\rho_2 \sigma_1^3 = 0.1$ ; the size ratio is  $\delta = 0.1$ . The horizontal line indicates the estimate of the squared localization length for large stars, defined as the inflection point of the MSD.

mass ratio is  $m_2/m_1 = 8.4 \times 10^{-3}$ , allowing an effective one-component description [31]. Indeed, the mean squared displacement in Fig. 5 shows a clear separation in time-scales between the two species. After the initial ballistic regime, the small stars simply become diffusive, while the large ones display a clear plateau, lasting about three decades in time, before eventually reaching the diffusive regime. Correspondingly, a difference in the diffusion coefficient (and relaxation time) of about three orders of magnitude is observed. By convention, we define the localization length as  $l_{MD} = \sqrt{\langle r^2(t^*) \rangle}$ , where  $t^*$  is the point of inflection of the MSD in the log – log plot. We therefore provide evidence that the large stars are nearly arrested in a jammed state, with a localization length that can be extracted from the plateau height  $l_{MD} \sim 0.25\sigma_1$  (horizontal line in Figure 5). A similar value could be extracted from a simulation of star polymers in theta-solvent [64]. Also our MCT results discussed provide a similar value, suggesting rather robustly that the localization length of a soft star glass is slightly higher than of the typical hard sphere one due to the softness of the cages which allows more flexibility in the rattling than in the case of rigid hard spheres.

We now turn to examine the density correlators. In Fig. 6, we show the behavior of  $\phi_{ii}(q, t)$  for large (a) and small stars (b) respectively for several wave vectors. As for the MSD, the large stars display a marked plateau at all wave vectors, lasting for about three decades in time. The height of the plateau oscillates as a function of the wave-vectors, as commonly found in standard glasses. We extract the non-ergodicity parameter of the system by fitting large stars  $\phi_{11}(q, t)$  with a stretched exponential law (Eq. 16). The results are shown in Fig. 7 together with the corresponding MCT predictions. We find that  $f_{11}(q)$  oscillates in phase with the static structure fac-



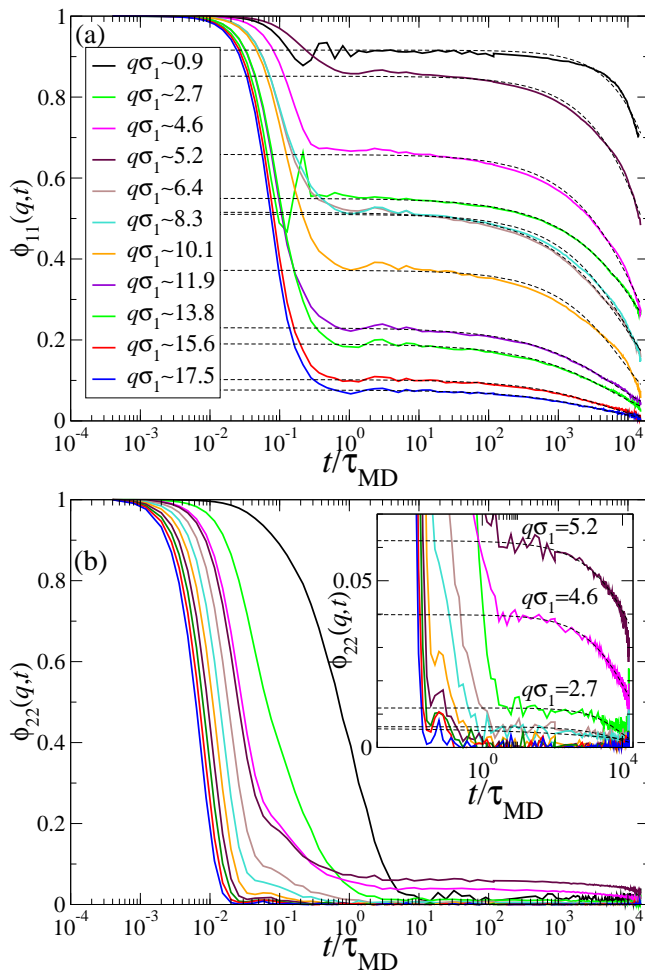


FIG. 6: Density correlators for large (a) and small (b) stars in the single class for different wave numbers  $q$  (see legends). The parameters are the same as in Fig. 5. The dashed lines are stretched exponential fits (Eq. (16)) to the curves. The inset (b) shows a magnification of the fits for  $q$ -values where small stars also display a two-step decay.

tor (not shown), but in contrast to the MCT predictions, it shows a marked increase at low  $q$ , while beyond the first peak the agreement is very good. We find that the stretching exponent  $\beta_q$  as a function of  $q\sigma_1$  also oscillates in phase with  $f_{11}(q)$ , and tends to approximately 0.6 for large  $q$ . Indeed, using this value as  $b$  exponent for the von Schweidler law (Eq. (15)), we find that all curves are well described in the region of departure from the plateau (Fig. 6(a)). This result for  $b$  agrees well with MCT predictions reported above. The estimates for  $f_{11}(q)$  from the von Schweidler fits are in perfect agreement with that obtained from the stretched exponential fits (Fig. 7).

For the small stars correlators (Fig. 6(b)), we find that the plateaus are sometimes so small that no accurate analysis can be performed. Nonetheless at small wave vectors, the stretched exponential fits work quite well (see inset). We find finite values  $f_{22}(q)$  just close to the first peak of  $S_{11}(q)$ , suggesting a confinement of the small

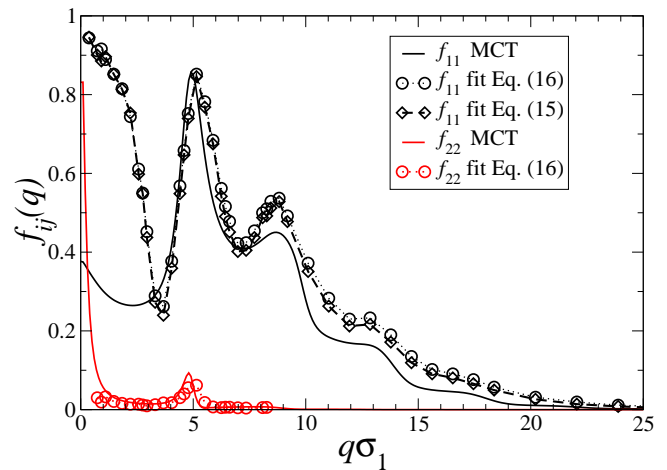


FIG. 7: Comparison of partial non-ergodicity parameters from MCT and simulation in the single glass. The values from the simulations are obtained by stretched exponential fits (Eq. (16)) for both types of stars. Also shown are results from von Schweidler fit (Eq. (15)) for large stars with  $b = 0.6$ . The simulation parameters are the same as in Fig. 5. The two component MCT results refer to the critical parameters:  $\rho_1\sigma_1^3 = 0.345$ ,  $\rho_2\sigma_1^3 = 0.12$  and  $\delta = 0.1$ .

stars in the frozen matrix of the large stars, which induces a small loss of ergodicity. Thus a coupling in time between large and small stars exists only at the peak of  $S_{11}(q)$ , which might explain why two-component MCT is still capable of correctly describing the general behavior of the mixture in this regime. The reason why the modes around  $q \approx 5\sigma_1^{-1}$  do not couple with modes at different  $q$  values is due to the fact that the structure factor of the small stars is structure-less except for this  $q$  value and close to the hydrodynamic limit ( $q \rightarrow 0$ ).

Theoretical descriptions of the dynamical arrest of a fluid in a frozen matrix have recently been developed [69, 70] which corresponds to the single glass state found here. Fig. 7 shows that  $f_{22}(q)$  is in good agreement with the MCT predictions, but we do not detect any increase of non-ergodicity at large length-scales. While MCT underestimates the non-ergodicity parameter of the large stars at low  $q$ , it overestimates the same for the small stars compared to the simulation results.

We can conclude from the combined study of MCT and simulations of the single glass that it corresponds to a glass formed by the large stars, whose properties are those typical of ultra-soft star polymer glasses. The presence of the small stars induces a weakening of the stability of the glass, until eventually melting it. We observe this in the behavior of the large stars' diffusion coefficient which grows with increasing density of the additives. The small stars are truly ergodic and fully mobile within the voids of the glassy matrix. They are never trapped in a metastable glass state. Nevertheless, they show a loss of ergodicity for length-scales of the order of the static structure factor first peak for the large stars. We remark that this behavior is seen both in binary MCT and

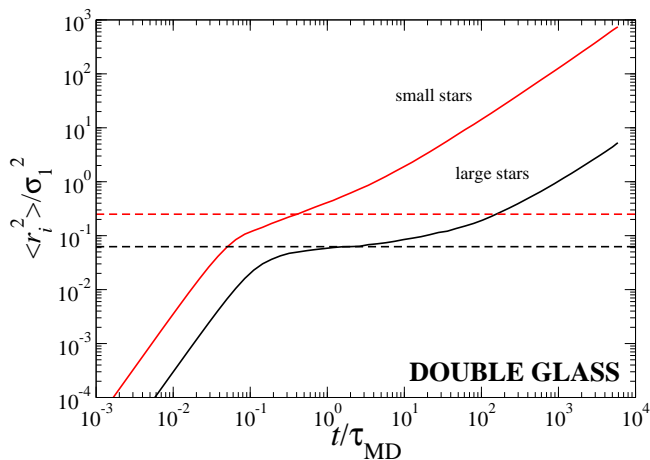


FIG. 8: Mean squared displacements for large and small stars in the double glass. The densities are  $\rho_1\sigma_1^3 = 0.41$  and  $\rho_2\sigma_1^3 = 0.1$ ; the size ratio is  $\delta = 0.4$ . The horizontal lines indicate the estimates of the squared localization length for large and small stars, respectively, defined as the inflection point of the MSD.

simulations, while it could not have been detected by an effective one-component treatment of large stars only.

### B. Region II: Double glass

We now turn to examine the arrested state for low  $\rho_2$  at large  $\delta$ . We consider the case  $\rho_1\sigma_1^3 = 0.41$ ,  $\delta = 0.4$  and  $\rho_2\sigma_1^3 = 0.1$ , so that the composition of the mixture is the same as for the single glass examined above. However, the additives are larger and, consequently, also their mass is larger. Here the mass ratio is  $m_2/m_1 = 8.5 \cdot 10^{-2}$ , which is one order of magnitude larger than in the single glass. Indeed, the simulations confirm an arrest of both species.

In Fig. 8, we show the MSD for both components in the mixture. Differently from the single case, we observe a significant slowing down also in the small component behavior, suggested by the intermediate time regime where the slope of  $\langle r_i^2 \rangle$  versus time (in the double-logarithmic plot) is smaller than 1, indicating a subdiffusive regime in the dynamics. In the same time window, the large stars are more confined than the small ones; their localization length  $l^{MD}$  remains equal to that of the single glass. For the small stars we can deduce instead a localization length of the order of  $0.5\sigma_1$ , about twice as large as that of the large stars, again in agreement with MCT predictions.

Looking at the partial density correlators for the double glass (Fig. 9(a)), we see a close similarity for the large stars correlators to those of the single glass. Only the time duration of the plateau changes, due to the different relative position of the chosen state point with respect to the glass transition. Indeed, it can be seen in Figs. 1 and 4 that this state point is ‘more liquid’ than the one we studied for the single glass. Similarly to the previ-

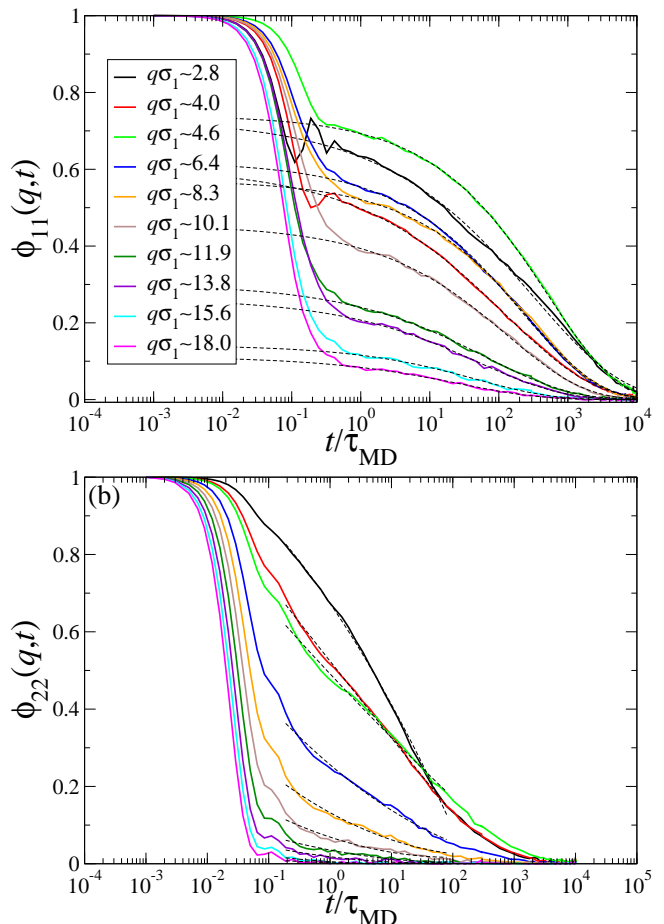


FIG. 9: Density correlators for large (a) and small (b) stars in the double glass for different values of wave number  $q$  (see legend). The parameters are the same as in Fig. 8. The dashed lines for the large stars are stretched exponential fits (Eq. (16)), while for the small stars we use logarithmic fits (Eq. (17)) with  $\tau/\tau_{MD} = 5$ .

ous paragraph, we can analyze the decay in terms of a stretched exponential and of a von Schweidler law and the results are totally equivalent to those of the single glass concerning dynamics of the large stars. The resulting  $f_{11}(q)$  is reported in Fig. 10 together with corresponding critical MCT predictions in this regime.

A completely different picture arises for the small stars (Fig. 9(b)). The density correlators cannot be described in terms of stretched exponentials. Indeed, they are best fitted with second order polynomial in  $\ln(t)$  of Eq. (17) with  $\tau/\tau_{MD} = 5$ . In other systems, this anomalous dynamical behavior has been attributed to the competition between two glassy states [55, 59, 60, 61, 71]. This seems to suggest the possible existence of a higher order MCT singularity [63], although we do not detect an increase of the exponent parameter  $\lambda$  in the MCT calculations. Interestingly, the logarithmic behavior is found only for the small stars, while the behavior of the large stars remains close to a standard liquid-glass transition or  $A_2$

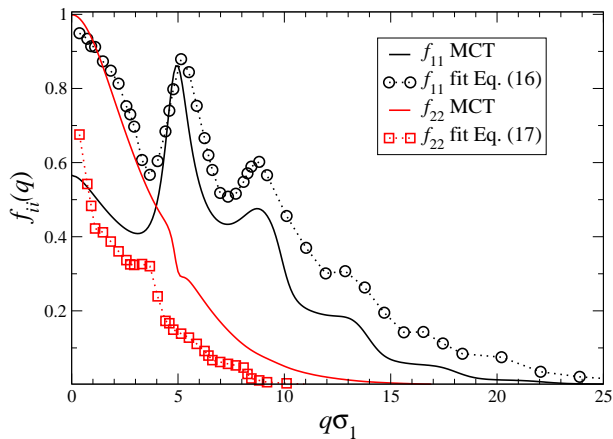


FIG. 10: Comparison of partial non-ergodicity parameters from MCT and simulation in the double glass. The values from the simulations are obtained by stretched exponential (Eq. (16)) fits for the large stars and from logarithmic (Eq. (17)) fits for the small stars. The simulation parameters are the same as in Fig. 8. The MCT results refer to the critical parameters:  $\rho_1\sigma_1^3 = 0.345$ ,  $\rho_2\sigma_1^3 = 0.05$  and  $\delta = 0.4$ .

singularity.

Performing the fits following Eq. (17), we extract a non-ergodicity parameter (Fig. 10) for the small component in good agreement with the one calculated within MCT close to the liquid-glass transition ( $\rho_2\sigma_1^3 = 0.05$ , see Fig. 1). Also, by looking at the  $h_q^{(2)}$  (not shown) extracted from the fits, we can find the wave vector  $q^*$  at which the decay is purely logarithmic [63, 72], which indicates the dominant length scale in the arrest process, and indeed it was estimated before for the attractive glass [55]. Here,  $h_q^{(2)} \sim 0$  for  $q\sigma_1 \approx 4$ , corresponding to a length-scale slightly larger than the nearest-neighbor length of the large stars, indicating that small stars are mostly trapped in the voids between large stars. Around this  $q^*$ -value there is the expected crossover between concave and convex shape for  $\phi_{22}(q, t)$  [63]. As for the single glass case, the estimates of  $f_{ii}(q)$  from the simulations differ from the MCT ones especially at low  $q$ , though the discrepancy is smaller in this case.

To summarize, the simulation results are in agreement with the MCT predictions discussed above, which suggest that the glassy properties of the large stars are identical in the single and double glass, both in terms of non-ergodicity parameter and localization length, while the small stars display a crossover from ergodic to arrested anomalous behavior.

### C. Region III: Asymmetric Glass

We analyze the state point  $\rho_1 = 0.345$ ,  $\rho_2\sigma_1^3 = 3.4$  and  $\delta = 0.4$  (5378 particles in the simulation), where the diffusivity decreases upon addition of small stars, as can be seen in Fig. 4.

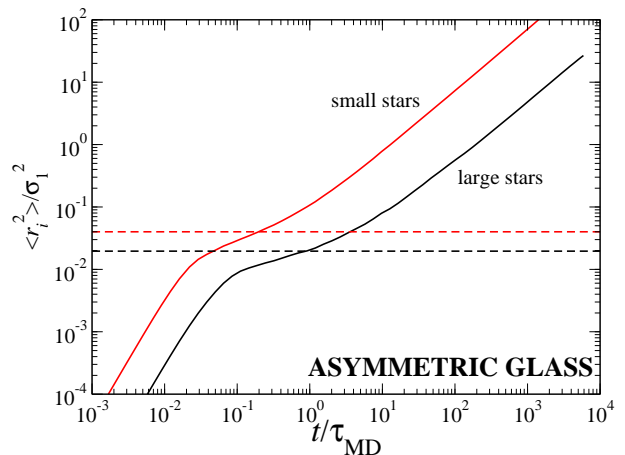


FIG. 11: Mean squared displacements for large and small stars in the asymmetric glass. The densities are  $\rho_1\sigma_1^3 = 0.345$  and  $\rho_2\sigma_1^3 = 3.4$ ; the size ratio is  $\delta = 0.4$ . The horizontal lines indicate the estimates of the squared localization length for large and small stars, respectively, defined as the inflection point of the MSD.

From the MSD reported in Fig. 11, we see that both components exhibit a slowing down in the dynamics, therefore we have evidence of a second state in which both components become arrested, i.e. a second double glass. However, the localization lengths that can be extracted from the MSD are smaller than those for the double glass discussed above. Indeed, we find  $l_{MD} \approx 0.14/\sigma_1$  for the large stars, corresponding to about half of the cage length that we found both in single and double glass, while  $l_{MD} \approx 0.2/\sigma_1$  for the small stars, again at least twice as small as that of the other (conventional) double glass. These values are again in remarkable agreement with those predicted by MCT. The additives do not only lead to a reduced localization length, but also deform the cages of the big particles, leading to an asymmetric glass [42].

The analysis of the density correlators provides evidence that the dynamics in this double asymmetric glass is very different from that of the standard double glass, see Fig. 12. Indeed, we cannot fit the correlators of the large stars with stretched exponentials, but rather they are found to follow the logarithmic decay of Eq. (17) with  $\tau/\tau_{MD} = 1$ . On the other hand, the small stars  $\phi_{22}(q, t)$  are well described by a stretched exponential decay for small wave vectors. The logarithmic behavior for large stars suggest the possibility of the presence of a higher order MCT singularity for the large stars or, at least, a competition between two different glassy states. Indeed, upon increasing  $\rho_2$  at fixed  $\delta = 0.4$ , the large stars are passing from the standard glass to a much more localized one. The same is true for the small stars in this region, so that a similar log-behavior is also expected for the small stars at some region of the phase diagram, but within the present study we are not able to detect that. However, we observe a deviation from standard stretched

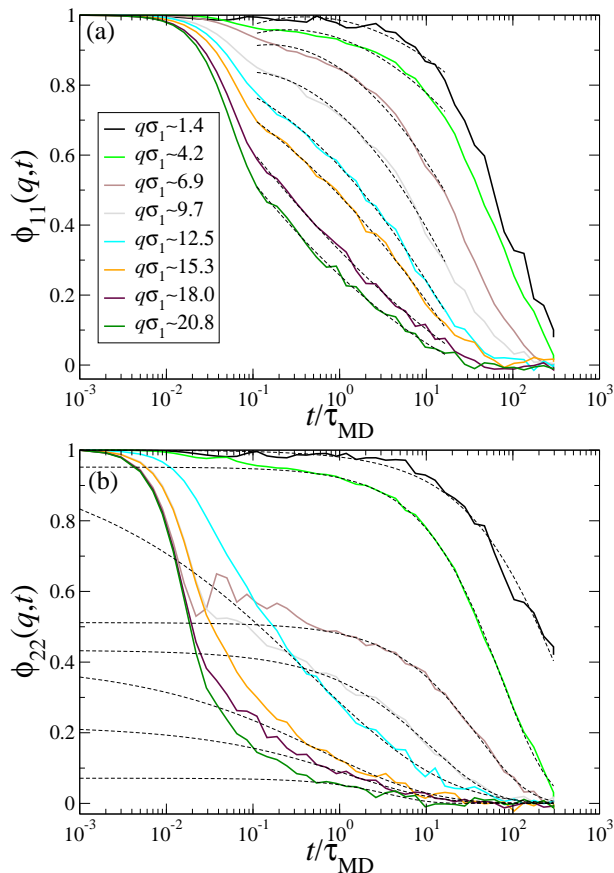


FIG. 12: Density correlators for large (a) and small (b) stars in the asymmetric for different wave numbers  $q$  (see legend). The parameters are the same as in Fig. 11. Here the large stars are described by polynomial in  $\ln(t)$  (Eq. (17)), for the small ones we use stretched exponentials (Eq. (16)).

exponential behavior at large  $q$  also for the small stars.

From the logarithmic fits for the large stars we determine the non-ergodicity parameters for large stars, again in quite good agreement with MCT predictions (see Fig. 13). Also, we can determine the  $q^*$  where the time dependence is logarithmic, i.e.  $q^*\sigma_1 \sim 16.6$ , thus invoking smaller length scales than the nearest-neighbor distance as responsible for the mechanism of arrest. We notice that this length is much larger than that found for attractive glasses in CP mixtures [55], consistent with the fact that here no attractive bonding is present. For the small stars, the stretched exponential fits are good at small wave-vectors, but become more uncertain for large  $q$  values. However, the fits show a satisfying agreement for the non-ergodicity parameters with the MCT predictions for the critical parameters  $\rho_1 = 0.345$ ,  $\rho_2 = 1.27$  and  $\delta = 0.4$ . We have also tried to use a Von Schweidler exponent  $b = 0.5$ , quite close to the MCT predictions, which also fits quite well the small stars correlators.

To recapitulate, also in the asymmetric glass we find good agreement between simulation results and MCT predictions. Moreover, we find again anomalous dynam-

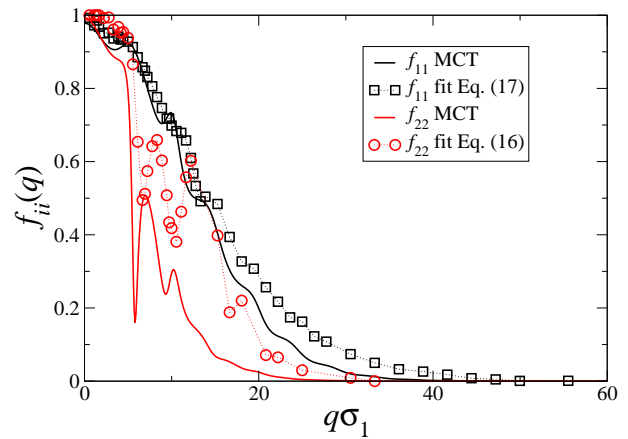


FIG. 13: Comparison of partial non-ergodicity parameters from MCT and simulation in the asymmetric glass. The values from the simulations are obtained by stretched exponential (Eq. (16)) fits for the small stars and from logarithmic (Eq. (17)) fits for the large stars with  $\tau/\tau_{MD} = 1$ . The simulation parameters are the same as in Fig. 11. The MCT results refer to the critical parameters:  $\rho_1\sigma_1^3 = 0.345$ ,  $\rho_2\sigma_1^3 = 1.27$  and  $\delta = 0.4$ .

ics. However, with respect to the double glass the properties of the small and large stars density correlators are reversed, i.e. now the large stars can be described in terms of stretched exponentials while the small ones exhibit a logarithmic decay. This fact, together with the growth of  $\lambda$  for this case as reported in the MCT results section, points to the possible existence of a nearby higher-order singularity for the large stars.

#### D. Region IV: Attractive Glass and Phase Separation

Finally, we turn to the region of small  $\delta$  and large  $\rho_2$  where we expect the occurrence of the attractive glass. However, this is difficult to observe due to competition with phase separation in the mixture. As already discussed before, we can only detect an attractive glass with binary MCT, because we are not able to observe a bending of the ideal glass line in the one-component MCT treatment before the integral equation calculations cease to converge.

Nevertheless, in the simulations, we do observe a decrease of the diffusion coefficient before the onset of phase separation (Fig. 14). After an initial increase of diffusivity the dynamics becomes slower with increasing  $\rho_2$ . However, this decrease is not sufficient to observe the emergence of a plateau in the MSD and to extract values for the nonergodicity parameter from the simulation.

We then used the static structure factor from the (monodisperse) simulations as input for the mode-coupling equations and detected a glassy state both in binary and one-component MCT for  $\rho_1\sigma_1^3 = 0.345$ ,  $\delta = 0.1$ , and  $\rho_2\sigma_1^3 = 20$ . The partial structure factors are shown in

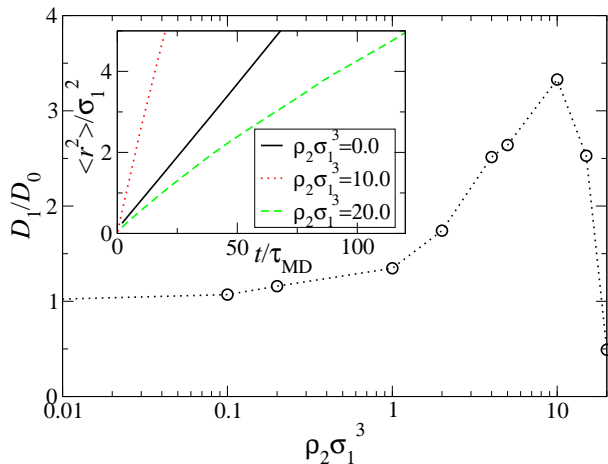


FIG. 14: Diffusion coefficient of the large stars, normalized by the value for the reference one-component system  $D_0$ , for  $\rho_1 \sigma_1^3 = 0.345$  and  $\delta = 0.1$  as a function of  $\rho_2$ . As an inset we show the MSD of the large stars for different concentrations of small ones.

Fig. 15(a). The small wave-length behavior of the structure factors shows the typical increase of a state point close to phase separation. In Fig. 15(b) we show the corresponding non-ergodicity parameters whose shape looks similar to the one found in previous studies of systems with attractive interactions [29]. It is interesting to note that the one- and two-component MCT give almost the same results for  $f_{11}(q)$ . Hence, the decrease of the diffusivity combined with large-scale fluctuations seems to indicate the possibility of an “arrested phase separation” [8] in this case, the interplay between glass transition and phase separation induces the dynamical arrest of the denser phase. This mechanism has been recently proposed to describe dynamical arrest at low and intermediate densities in CP mixtures [73] and other attractive systems [74].

## VII. CONCLUSIONS

In conclusion, we have identified different glassy states in a binary mixture of star polymers by using extensive computer simulations and mode coupling theory. In the plane spanned by size asymmetry between the two components and concentration of the added small star, there is a liquid lake which reveals multiple reentrant behaviors. Both the upper and lower threshold concentrations for the liquid-glass transition behave nonmonotonically with the size asymmetry  $\delta$ . At high concentrations  $\rho_2$  of small stars and  $\delta = 0.4$ , we have identified a new, asymmetric double glass type which is characterized by a strong localization of the small particles and anisotropic cages. This is different both from the usual double glass at low concentrations  $\rho_2$  and from the hard sphere double glass [33]. Recent experiments confirm our theoretical findings [42]. At low  $\delta$  and high  $\rho_2$  there is a competi-

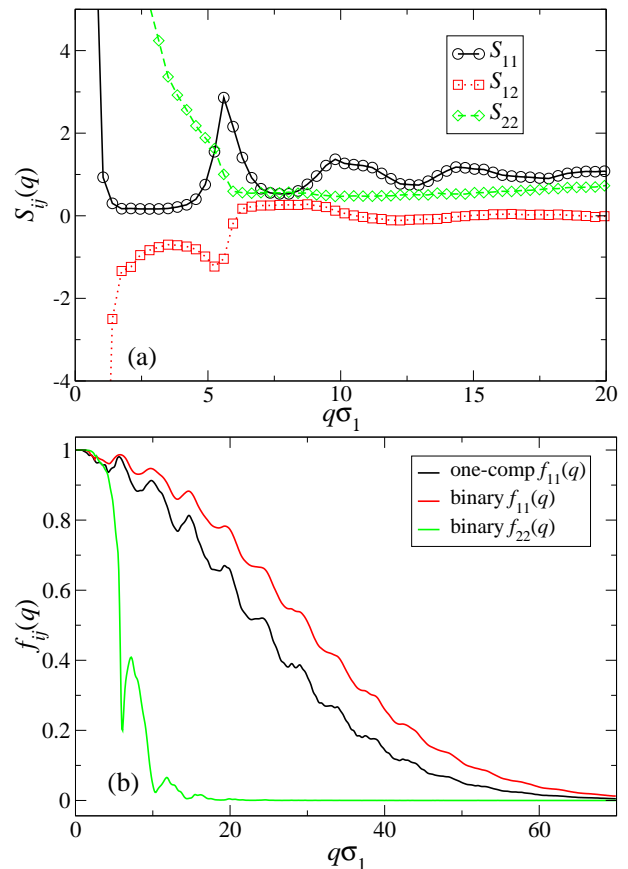


FIG. 15: (a) Partial structure factors  $\rho_1 \sigma_1^3 = 0.345$ ,  $\delta = 0.1$ , and  $\rho_2 \sigma_1^3 = 20$ . Note the small- $q$  behavior of all three curves, which signals phase separation. (b) The corresponding non-ergodicity parameters predicted by MCT.

tion between vitrification and phase separation. In all the explored phase space, we find remarkable agreement between simulation results and MCT predictions.

An interesting open question is which minimum arm numbers  $f_1$  and  $f_2$  are necessary for the formation of a high- $\rho_2$  glass, as we know that one-component star polymer systems with less than  $\approx 40 - 45$  arms do not ever glassify [34]. An additional interesting question concerns the presence of higher order singularities in the wide parameter space that can be explored with star-polymer binary mixtures. Indeed, the MD results provide evidence of a non-conventional slowing down of the dynamics in the proximity of the double and of the asymmetric glass. It is important to find out if MCT predicts any sharp glass-glass transition between single and double glass, or between double and asymmetric glass. This will be the subject of a future study. A more exhaustive theoretical study is requested to properly map the MCT results with the numerical ones and provide a guide-line for locating, if existing, the higher order singularities, similarly to what has been done for the case of short-range attractive colloids[55, 72].

### Acknowledgments

The authors thank E. Stiakakis, D. Vlassopoulos, and I. Saika-Voivod for many helpful discussions. This work has been supported by the DFG within the SFB-TR6, by MIUR PRIN and by the EU within the Network of Excellence “Softcomp” and the Marie Curie Research and Training Network “Dynamical Arrested States of Soft

Matter and Colloids” (MRTN-CT-2003-504712). C.M. thanks the Alexander von Humboldt Foundation for financial support. C.N.L. thanks the Erwin Schrödinger Institute (ESI) in Vienna for a Senior Research Fellowship as well as the ESI and the Vienna University of Technology, where parts of this work have been carried out, for their hospitality.

- 
- [1] Pusey, P. N. Liquids, Freezing and the Glass Transition, in *Les Houches Summer Schools of Theoretical Physics Session LI (1989)*, edited by J.P. Hansen, D. Levesque, and J. Zinn-Justin, North-Holland Amsterdam, 1991.
- [2] Cipelletti, L.; Ramos, L. *J. Phys.: Condens. Matter* **2005**, *17*, R253.
- [3] Berthier, L.; Biroli, G.; Bouchaud, J. P.; Cipelletti, L.; El Masri, D.; L'Hôte, D.; Ladieu, F.; M. Pierno, M. *Science* **2005**, *310*, 1797.
- [4] Barrat, J. L.; Klein, M. L. *Ann. Rev. Phys. Chem.* **1991**, *42*, 23.
- [5] Mischler, C.; Baschnagel, J.; Binder, K. *Adv. Colloid Interface Sci.* **94**, 197 (2001).
- [6] Baschnagel, J.; Varnik, F. *J. Phys.: Condens. Matter* **2005**, *17*, R851.
- [7] Sciortino, F.; Tartaglia, P. *Adv. Phys.* **2005**, *54*, 471.
- [8] Zaccarelli, E. *J. Phys.: Condens. Matter* **2007**, *19*, 323101.
- [9] Heuer, A. *J. Phys.: Condens. Matter* **2008**, in press.
- [10] W. Götze, Liquids, Freezing and the Glass Transition, in *Les Houches Summer Schools of Theoretical Physics Session LI (1989)*, edited by J.P. Hansen, D. Levesque, and J. Zinn-Justin, pp. 287–503, North-Holland Amsterdam, 1991.
- [11] Götze, W. *J. Phys.: Condens. Matter* **1999**, *11*, A1.
- [12] Garrahan, J. P.; Chandler, D. *Phys. Rev. Lett.* **2002**, *89*, 035704.
- [13] Schweizer, K. S. *J. Chem. Phys.* **2007**, *127*, 164506.
- [14] Kob, W.; Andersen, H. C. *Phys. Rev. Lett.* **1994**, *73*.
- [15] Likos, C. N.; Henley, C. L. *Phil. Mag. B* **1993**, *68*, 85.
- [16] Fernandez, J. R.; Harrowell, P. *J. Chem. Phys.* **2004**, *120*, 9222.
- [17] Fornleitner, J.; Lo Verso, F.; Kahl, G.; Likos, C. N. *Soft Matter* **2008**, *4*, 480.
- [18] Roux, J. N.; Barrat, J. L.; Hansen, J.-P. *J. Phys.: Condens. Matter* **1989**, *1*, 7171.
- [19] Barrat, J.-L.; Latz, A. *J. Phys.: Condens. Matter* **1990**, *2*, 4289.
- [20] Bordat, P.; Affouard, F.; Descamps, M.; Ngai, K. L. *J. Non.-Cryst. Solids* **2006**, *352*, 4630.
- [21] Vollmayr-Lee, K.; Baker, E. A. *Europhys. Lett.* **2006**, *76*, 1130.
- [22] Fernandez, J. R.; Harrowell, P. *Phys. Rev. E* **2003**, *67*, 011403.
- [23] Bosse, J.; Wilke, S. D. *Phys. Rev. Lett.* **1998**, *80*, 1260.
- [24] Doliwa, B.; Heuer, A. *Phys. Rev. Lett.* **1998**, *80*, 4915.
- [25] Löwen, H.; Hansen, J. P.; Roux, J. N. *Phys. Rev. A* **1991**, *44*, 1169.
- [26] Zaccarelli, E.; Andreev, S.; Sciortino, F.; Reichman, D. R. *Phys. Rev. Lett.* **2008**, *100*, 195701.
- [27] Pham, K. N.; Puertas, A. M.; Bergenholtz, J.; Egelhaaf, S. U.; Moussaïd, A.; Pusey, P. N.; Schofield, A. B.; Cates, M. E.; Fuchs, M.; Poon, W. C. K. *Science* **2002**, *296*, 104.
- [28] Zaccarelli, E.; Foffi, G.; Dawson, K. A.; Sciortino, F.; Tartaglia, P. *Phys. Rev. E* **2001**, *63*, 031501.
- [29] Bergenholtz, J.; Fuchs, M. *Phys. Rev. E* **1999**, *59*, 5706.
- [30] Sciortino, F. *Nature Materials* **2002**, *1*, 145.
- [31] Zaccarelli, E.; Löwen, H.; Wessels, P. P. F.; Sciortino, F.; Tartaglia, P.; Likos, C. N. *Phys. Rev. Lett.* **2004**, *92*, 225703.
- [32] Imhof, A.; Dhont, J. K. G. *Phys. Rev. Lett.* **1995**, *75*, 1662.
- [33] Foffi, G.; Götze, W.; Sciortino, F.; Tartaglia, P.; Voigtmann, T. *Phys. Rev. E* **2004**, *69*, 011505.
- [34] Foffi, G.; Sciortino, F.; Tartaglia, P.; Zaccarelli, E.; Lo Verso, F.; Reatto, L.; Dawson, K. A.; Likos, C. N. *Phys. Rev. Lett.* **2003**, *90*, 238301.
- [35] Loppinet, B.; Stiakakis, E.; Vlassopoulos, D.; Fytas, G.; Roovers, J. *Macromolecules* **2001**, *34*, 8216.
- [36] Laurati, M.; Stellbrink, J.; Lund, R.; Willner, L.; Richter, D.; Zaccarelli, E. *Phys. Rev. Lett.* **2005**, *94*, 195504.
- [37] Laurati, M.; Stellbrink, J.; Lund, R.; Willner, L.; Zaccarelli, E.; Richter, D. *Phys. Rev. E* **2007**, *76*, 041503.
- [38] Zaccarelli, E.; Mayer, C.; Asteriadi, A.; Likos, C. N.; Sciortino, F.; Roovers, J.; Iatrou, H.; Hadjichristidis, N.; Tartaglia, P.; Löwen, H.; Vlassopoulos, D. *Phys. Rev. Lett.* **2005**, *95*, 268301.
- [39] Likos, C. N.; Löwen, H.; Watzlawek, M.; Abbas, B.; Jucknische, O.; Allgaier, J.; Richter, D. *Phys. Rev. Lett.* **1998**, *80*, 4450.
- [40] Stiakakis, E.; Vlassopoulos, D.; Likos, C. N.; Roovers, J.; Meier, G. *Phys. Rev. Lett.* **2002**, *89*, 1.
- [41] Mayer, C.; Likos, C. N. *Macromolecules* **2007**, *40*, 1196.
- [42] Mayer, C.; Zaccarelli, E.; Stiakakis, E.; Likos, C. N.; Sciortino, F.; Munam, A.; Gauthier, M.; Hadjichristidis, N.; Iatrou, H.; Tartaglia, P.; Löwen, H.; Vlassopoulos, D. *Nat. Mat.* **2008**, *7*, 780.
- [43] von Ferber, C.; Jusufi, A.; Watzlawek, M.; Likos, C. N.; Löwen, H. *Phys. Rev. E* **2000**, *62*, 6949.
- [44] Hansen, J.-P.; MacDonald, I. R. *Theory of Simple Liquids*, Academic: London, 3rd edition, 2006.
- [45] Rogers, F. J.; Young, D. A. *Phys. Rev. A* **1984**, *30*, 999.
- [46] Mayer, C.; Likos, C. N.; Löwen, H. *Phys. Rev. E* **2004**, *70*, 041402.
- [47] Watzlawek, M.; Löwen, H.; Likos, C. N. *J. Phys.: Condens. Matter* **1998**, *10*, 8189.
- [48] Kumar, P.; Buldyrev, S. V.; Sciortino, F.; Zaccarelli, E.; Stanley, H. E. *Phys. Rev. E* **2005**, *72*, 021501.
- [49] Lang, A.; Kahl, G.; Likos, C. N.; Löwen, H.; Watzlawek, M. *J. Phys.: Condens. Matter* **1999**, *11*, 10143.

- [50] Mayer, C.; Stiakakis, E.; Zaccarelli, E.; Likos, C. N.; Sciortino, F.; Tartaglia, P.; Löwen, H.; Vlassopoulos, D. *Rheol. Acta* **2007**, *46*, 611.
- [51] Götze, W; Voigtmann, T. *Phys. Rev. E* **2003**, *67*, 021502.
- [52] Thakur, J. S.; Bosse, J. *Phys. Rev. A* **1991**, *43*, 4388.
- [53] Thakur, J. S.; Bosse, J. *Phys. Rev. A* **1991**, *43*, 4378.
- [54] Dawson, K. A.; Foffi, G.; Fuchs, M.; Götze, W.; Sciortino, F.; Sperl, M.; Tartaglia, P.; Voigtmann, T.; Zaccarelli, E. *Phys. Rev. E* **2001**, *63*, 011401.
- [55] Sciortino, F.; Tartaglia, P.; Zaccarelli, E. *Phys. Rev. Lett.* **2003**, *91*, 268301.
- [56] Zaccarelli, E.; Foffi, G.; Sciortino, F.; Tartaglia, P. *Phys. Rev. Lett.* **2003**, *91*, 108301.
- [57] Eckert, T; Bartsch, E. *Phys. Rev. Lett.* **2002**, *89*, 125701.
- [58] Grandjean, J.; Mourchid, A. *Europhys. Lett.* **2004**, *65*, 712.
- [59] Moreno, A. J.; Colmenero, J. *J. Chem. Phys.* **2006**, *125*, 016101.
- [60] Moreno, A. J.; Colmenero, J. *Phys. Rev. E* **74**, 021409 (2006).
- [61] Moreno, A. J.; Colmenero, J. *J. Chem. Phys.* **2006**, *125*, 164507.
- [62] Fuchs, M. *J. Non-Cryst. Solids* **1994**, *172*, 241.
- [63] Götze, W; Sperl, M. *Phys. Rev. E* **2002**, *66*, 011405.
- [64] Rissanou, A. N.; Vlassopoulos, D; Bitsanis, I. A. *Phys. Rev. E* **2005**, *71*, 011402.
- [65] Gleim, T.; Kob, W.; K. Binder, K. *Phys. Rev. Lett.* **1998**, *81*, 4404.
- [66] Likos, C. N. *Phys. Rep.* **2001**, *348*, 261.
- [67] Grest, G. S.; Fetters, L. J.; Huang, J. S.; Richter, D. *Adv. Chem. Phys.* **1996**, *XCIV*, 67.
- [68] Zaccarelli, E.; Foffi, G.; Dawson, K. A.; Buldyrev, S. V.; Sciortino, F.; Tartaglia, P. *Phys. Rev. E* **2002**, *66*, 041402.
- [69] Krakoviack, V. *Phys. Rev. Lett.* **2007**, *94*, 065703.
- [70] Juárez-Maldonado, R.; Medina-Noyola, M. *Phys. Rev. E* **2008**, *77*, 051503.
- [71] Zaccarelli, E.; Saika-Voivod, I.; Moreno, A. J.; Buldyrev, S. V.; Tartaglia, P. Sciortino, F. *J. Chem. Phys.* **2006**, *124*, 124908.
- [72] Sperl, M. *Phys. Rev. E* **2004**, *69*, 011401.
- [73] Lu, P. J.; Zaccarelli, E.; Ciulla, F.; Schofield, A. B.; Sciortino, F.; Weitz, D. A. *Nature* **2008**, *453*, 499.
- [74] Cardinaux, F.; Gibaud, T.; Stradner, A.; Schurtenberger, P. *Phys. Rev. Lett.* **2007**, *99*, 118301.
- [75] MCT long-time limit equations are solved iteratively discretizing the wave vector integrals on a grid of 1000 points for the binary equations (Eq.11) and 1600 for the one-component ones (Eq.9), with a mesh in wave vectors respectively of  $0.1/\sigma_1$  and  $0.0625/\sigma_1$ .